Peptidylglycine α-amidating monooxygenase is required for atrial secretory granule formation

Nils Bäck[a] , Raj Luxmi[b] , Kathryn G. Powers[c] , Richard E. Mains[c] , and Betty A. Eipper[b,c,1]

[a]Department of Anatomy, University of Helsinki, 00100 Helsinki, Finland; [b]Department of Molecular Biology & Biophysics, University of Connecticut Health Center, Farmington, CT 06030; and [c]Department of Neuroscience, University of Connecticut Health Center, Farmington, CT 06030

The discovery of atrial secretory granules and the natriuretic peptides stored in them identified the atrium as an endocrine organ. Although neither atrial nor brain natriuretic peptide (ANP, BNP) is amidated, the major membrane protein in atrial granules is peptidylglycine α-amidating monooxygenase (PAM), an enzyme essential for amidated peptide biosynthesis. Mice lacking cardiomyocyte PAM ($Pam^{Myh6\text{-}cKO/cKO}$) are viable, but a gene dosage-dependent drop in atrial ANP and BNP content occurred. Ultrastructural analysis of adult $Pam^{Myh6\text{-}cKO/cKO}$ atria revealed a 13-fold drop in the number of secretory granules. When primary cultures of $Pam^{0\text{-}Cre\text{-}cKO/cKO}$ atrial myocytes (no Cre recombinase, PAM floxed) were transduced with Cre-GFP lentivirus, PAM protein levels dropped, followed by a decline in ANP precursor (proANP) levels. Expression of exogenous PAM in $Pam^{Myh6\text{-}cKO/cKO}$ atrial myocytes produced a dose-dependent rescue of proANP content; strikingly, this response did not require the monooxygenase activity of PAM. Unlike many prohormones, atrial proANP is stored intact. A threefold increase in the basal rate of proANP secretion by $Pam^{Myh6\text{-}cKO/cKO}$ myocytes was a major contributor to its reduced levels. While proANP secretion was increased following treatment of control cultures with drugs that block the activation of Golgi-localized Arf proteins and COPI vesicle formation, proANP secretion by $Pam^{Myh6\text{-}cKO/cKO}$ myocytes was unaffected. In cells lacking secretory granules, expression of exogenous PAM led to the accumulation of fluorescently tagged proANP in the cis-Golgi region. Our data indicate that COPI vesicle-mediated recycling of PAM from the cis-Golgi to the endoplasmic reticulum plays an essential role in the biogenesis of proANP containing atrial granules.

atrial natriuretic peptide | PAM | ultrastructure | secretion | golgicide A

In response to stretch, sympathetic input, and hormones like endothelin-1, atrial myocytes release natriuretic peptides essential for fluid volume homeostasis (1, 2). The proatrial natriuretic peptide (proANP)-containing granules in atrial myocytes, which look much like the granules in insulin-producing β-cells and proopiomelanocortin (POMC)-producing corticotropes, exhibit important differences. Atrial granules accumulate near the Golgi complex and store their major product, proANP, intact. The subtilisin-like endoproteases responsible for producing product peptides from inactive precursors in neurons and endocrine cells are not expressed in cardiomyocytes (3). Instead, Corin cleaves proANP at the time of secretion (1, 2, 4). While calcium influx or intracellular release plays a major role in the stimulated secretion of islet, pituitary, and chromaffin cell hormones, it is not essential for atrial proANP secretion (5, 6). Specific aspects of the secretion of many peptide hormones (7–9) are inhibited by Brefeldin A (BFA), a fungal metabolite that inhibits the Golgi-localized GDP/GTP exchange factors (GEFs) that activate Arf family GTP-binding proteins (10–12). In contrast, atrial myocyte secretion of ANP is stimulated by BFA (13, 14).

Natriuretic peptides, proANP and probrain natriuretic peptide (proBNP), are the major atrial granule content proteins. Granule membrane proteins play essential roles in granule formation and maturation, cargo protein posttranslational processing, luminal pH maintenance, ion transport, and cytoskeletal interactions.

Strikingly, peptidylglycine α-amidating monooxygenase (PAM), a type I transmembrane enzyme that converts peptidylglycine substrates (luminal peptides with a COOH-terminal Gly) into amidated products, is the major atrial granule membrane protein (15, 16). For many neuroendocrine peptides, amidation is essential to function (17). However, neither ANP nor BNP is amidated, suggesting that PAM performs a noncatalytic, structural role in atrial granules (15, 16). In support of this idea, PAM has been reported to interact with proANP in a manner dependent on the proANP calcium-binding site (18).

Genetic studies have linked both *NPPA* (which encodes proANP) and *PAM* to heart disease. A mutation in *NPPA* was identified as a causative factor in familial, early onset atrial fibrillation (19). In isolated atrial amyloidosis, which is associated with congestive heart failure and atrial fibrillation, ANP and its N-terminal fragment are major amyloid fibril components (20). PAM has been identified as a risk factor for type 2 diabetes (21, 22), coronary heart disease (21, 23), and hypertension (24). Although atrial fibrillation, the most common arrhythmia in the elderly and a leading cause of stroke, is accompanied by changes in the organization of the Golgi complex and microtubule network in atrial myocytes (25–27), our limited understanding of the unique features of these cells limits our ability to manipulate them in a therapeutically useful manner.

Mice unable to express PAM in cardiomyocytes were generated by crossing mice expressing a floxed allele of *Pam* ($Pam^{0\text{-}Cre\text{-}cKO/cKO}$) to mice expressing Cre recombinase under control of the myosin heavy chain 6 (*Myh6*) promoter (3, 28). $Pam^{Myh6\text{-}cKO/cKO}$ mice have

Significance

Transmission electron microscopy of atrial cardiomyocytes revealed dense granules resembling those in endocrine cells and neurons, leading to the discovery of the natriuretic peptides stored in these granules. Subsequent studies revealed features unique to atrial granules, including high-level expression of peptidylglycine α-amidating monooxygenase (PAM), an enzyme required for the synthesis of many neuropeptides, but not for the synthesis of natriuretic peptides. The discovery that atrial myocytes lacking PAM are unable to produce granules and that PAM lacking its monooxygenase activity can rescue granule formation provides new information about the proANP secretory pathway. A better understanding of the unique features of atrial cell biology should provide insight into atrial fibrillation, the most common cardiac arrhythmia, atrial amyloidosis, and heart failure.

www.manaraa.com

dramatically reduced levels of proANP in their atria and mature ANP in their sera (3). These decreases cannot be attributed to a decline in *Nppa* mRNA levels. We used ultrastructural, biochemical, and pharmacological approaches to demonstrate the inability of *Pam*[Myh6-cKO/cKO] atrial myocytes to store selected soluble cargo proteins in granules. Our exploration of the underlying mechanism highlighted unique features of the secretory pathway in atrial myocytes, revealing a role for PAM in prolonging the half-life of proANP by protecting it from basal secretion and degradation.

Results

Secretory Granules Are Rarely Seen in the Atria of *Pam*[Myh6-cKO/cKO] Mice.

We turned to transmission electron microscopy to determine whether the decreased proANP levels observed in *Pam*[Myh6-cKO/cKO] atria (3) were accompanied by a decrease in secretory granule (SG) number. Perinuclear Golgi complexes and nearby SGs were readily observed in control myocytes (Fig. 1*A* and *SI Appendix*, Fig. S1 *A and C*). Although perinuclear Golgi complexes were present in *Pam*[Myh6-cKO/cKO] atria, SGs were rarely observed in their vicinity (Fig. 1*B* and *SI Appendix*, Fig. S1 *B and D*). To search for SGs localized elsewhere in *Pam*[Myh6-cKO/cKO] atria (*SI Appendix*, Fig. S1 *E and F*), randomly oriented tissue blocks from the left atria of three wild-type and three *Pam*[Myh6-cKO/cKO] mice were systematically examined (*Methods*). Myocyte cell size was not altered when expression of PAM was eliminated; myocyte cell width did not differ in control and *Pam*[Myh6-cKO/cKO] atria (5.7 ± 0.1 and 6.1 ± 0.1 μm, respectively); nuclear volume fraction was unaltered (3.6 ± 0.5% in control and 2.8 ± 0.5% in *Pam*[Myh6-cKO/cKO] cells).

Unbiased sampling of all parts of the cytoplasm allowed morphometric analysis of the cytoplasmic volume fraction occupied by specific organelles; sections were photographed at 25-μm intervals (4,000×) from a random start (6). Myofilaments and mitochondria, which fill most of the cytoplasmic volume (29), were unaltered. Morphometric analysis of the cytoplasmic volume occupied by the Golgi complex, SGs, multivesicular bodies (MVBs), and lysosomes revealed a 20-fold decrease in SG cytoplasmic volume in *Pam*[Myh6-cKO/cKO] cardiomyocytes (Fig. 1*C*).

The number of SGs observed in transections of the Golgi complex dropped 13-fold in *Pam*[Myh6-cKO/cKO] atria (Fig. 1*D*), exceeding the 3-fold drop in their proANP content. In control atrial myocytes, granules located in the perinuclear Golgi region had a larger diameter than peripherally localized granules (Fig. 1*E*). The granules in the perinuclear Golgi region in *Pam*[Myh6-cKO/cKO] myocytes had smaller diameters than similarly localized granules in control cells, and their diameters did not differ from peripherally localized granules. The mean transection diameter of all SGs, regardless of localization, was 171 ± 1 nm in control atrial myocytes and 147 ± 5 nm in *Pam*[Myh6-cKO/cKO] atrial myocytes: The 14.0% decrease in the transection diameter of SGs in *Pam*[Myh6-cKO/cKO] myocytes corresponds to a 36.5% decrease in granule volume. Taking this into account, the 20-fold decrease in the cytoplasmic volume fraction occupied by SGs in *Pam*[Myh6-cKO/cKO] cardiomyocytes corresponds to a 13-fold drop in the number of SGs per cell, as observed for Golgi-localized granules. Irregularly shaped granules (Fig. 1 *B, Inset*) were more common in the perinuclear Golgi region of *Pam*[Myh6-cKO/cKO] atria than in control atria (52.7 ± 4.0% of the granules in *Pam*[Myh6-cKO/cKO] atria vs. 11.7 ± 0.7% in control atria; ± SEM, $P < 0.001$).
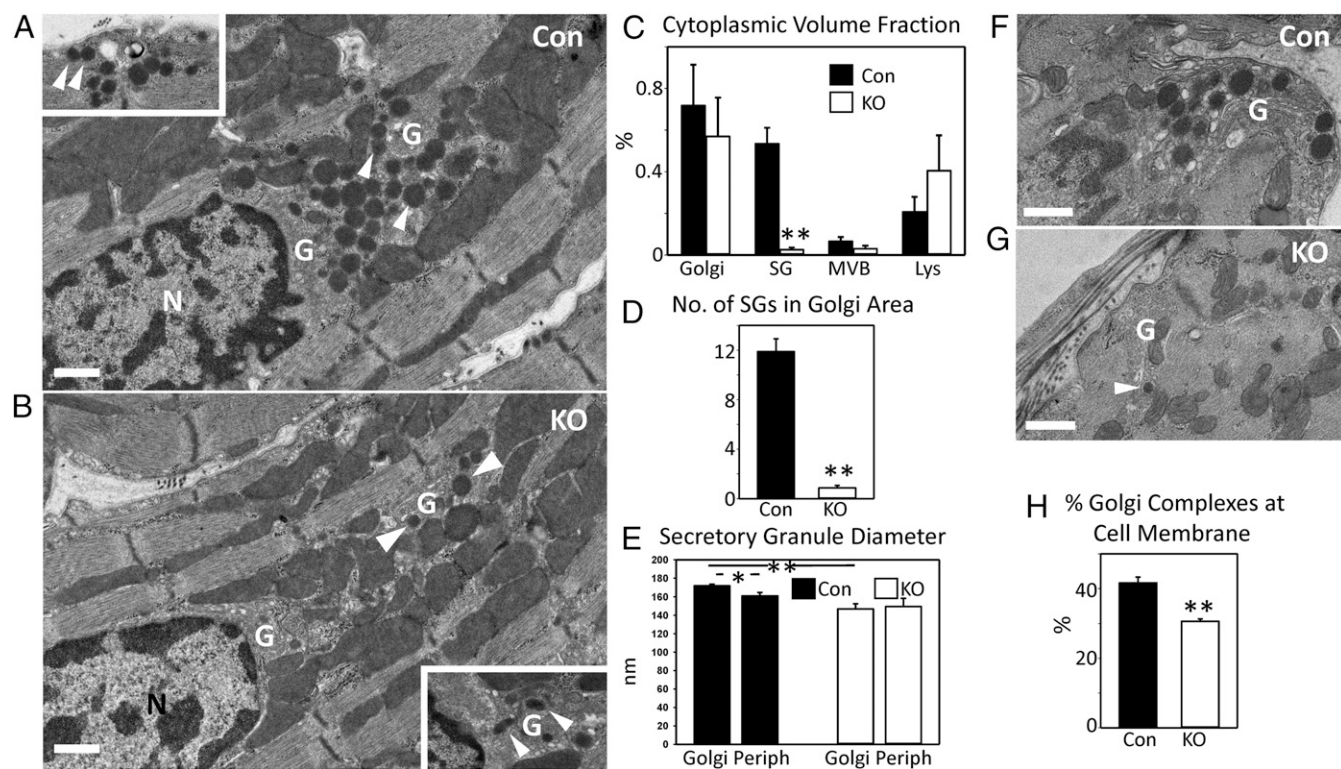
Fig. 1. SGs are rarely seen in the atria of *Pam*[Myh6-cKO/cKO] mice. Images of control (Con) (*A*) and *Pam*[Myh6-cKO/cKO] (*B*) atria including nucleus (N) and Golgi (G) complex; SGs are marked with arrowheads. *Inset* in *A* shows SGs at the cell periphery. *Inset* in *B* shows Golgi membranes and irregular SGs. Quantification of cytoplasmic volume fractions for Golgi, SGs, MVB, and lysosomes (Lys) (*C*), SG number in sections including the Golgi complex (Golgi membranes bordered by mitochondria and myofilament bundles) (*D*), and SG diameter in sections including the Golgi or peripheral membranes (*E*) in control and *Pam*[Myh6-cKO/cKO] (KO) atria. (*F* and *G*) Images of Golgi complexes at the cell membrane in control and *Pam*[Myh6-cKO/cKO] atria. Arrowhead in *G* shows an SG. (*H*) Quantification of the percentage of Golgi complexes at the cell membrane. In *C–E*, **$P < 0.001$ and *$P < 0.05$. In *H*, **$P < 0.005$. (Scale bars, 500 nm.)

Bäck et al.

Golgi membranes were also observed near the periphery of control and $Pam^{\text{Myh6-cKO/cKO}}$ myocytes (Fig. 1 *F* and *G*) (25). In control cells, 40% of the Golgi membranes were located near the cell surface; a smaller percentage of the Golgi complexes were located near the cell membrane in $Pam^{\text{Myh6-cKO/cKO}}$ myocytes (Fig. 1*H*). As for perinuclear Golgi complexes, SGs were prevalent near peripheral Golgi complexes in control cells but were rarely observed in this region in $Pam^{\text{Myh6-cKO/cKO}}$ myocytes.

Golgi-Localized Lysosomes Are Smaller in the Atria of $Pam^{\text{Myh6-cKO/cKO}}$ Mice. In pituitary cells, PAM that reaches the plasma membrane is retrieved via clathrin-mediated endocytosis and is either recycled to SGs or degraded (30, 31). The endocytic trafficking of PAM is regulated and involves its entry into the intraluminal vesicles of MVBs. For this reason, we examined MVBs in control and $Pam^{\text{Myh6-cKO/cKO}}$ atrial myocytes. In both genotypes, MVBs were observed near the Golgi complex and SGs (Fig. 2 *A–D*, arrowheads). Irregularly shaped, dark staining lysosomes were seen close to the Golgi complex in both control and $Pam^{\text{Myh6-cKO/cKO}}$ atrial myocytes (Fig. 2 *E* and *F*). Residual bodies, which release membranous aggregates, did not vary with genotype (Fig. 2*G*, arrowheads). In both control and $Pam^{\text{Myh6−cKO/cKO}}$ myocytes, MVBs containing electron-dense material resembling the cores of SG were occasionally observed (Fig. 2 *H* and *I*), consistent with the occurrence of crinophagy (32).

The fraction of Golgi complex transections containing MVBs or lysosomes did not differ in control and $Pam^{\text{Myh6-cKO/cKO}}$ myocytes (Fig. 2*J*). The diameters of peripheral and Golgi-localized MVBs, peripheral lysosomes, and residual bodies did not differ based on genotype, but Golgi-localized lysosomes were smaller in $Pam^{\text{Myh6-cKO/cKO}}$ myocytes (Fig. 2*K*); the observed decrease in diameter would account for a threefold drop in the volume of Golgi-localized lysosomes. The peripheral rim of cytoplasm was filled with an extensive array of invaginations, vesicles, and tubules (Fig. 2 *L* and *M*). Ultrastructurally, it was not possible to distinguish T-tubules, sarcoplasmic reticulum (SR), caveolae, and endocytic vesicles. The volume fraction of these structures was identical in control and $Pam^{\text{Myh6-cKO/cKO}}$ cardiomyocytes ($0.96 \pm 0.19\%$ and $0.95 \pm 0.29\%$, respectively). Based on an unbiased transmission electron microscopic analysis of secretory pathway organelles in atrial myocytes from control and $Pam^{\text{Myh6-cKO/cKO}}$ mice, the major difference was the almost total absence of atrial granules in myocytes lacking PAM.
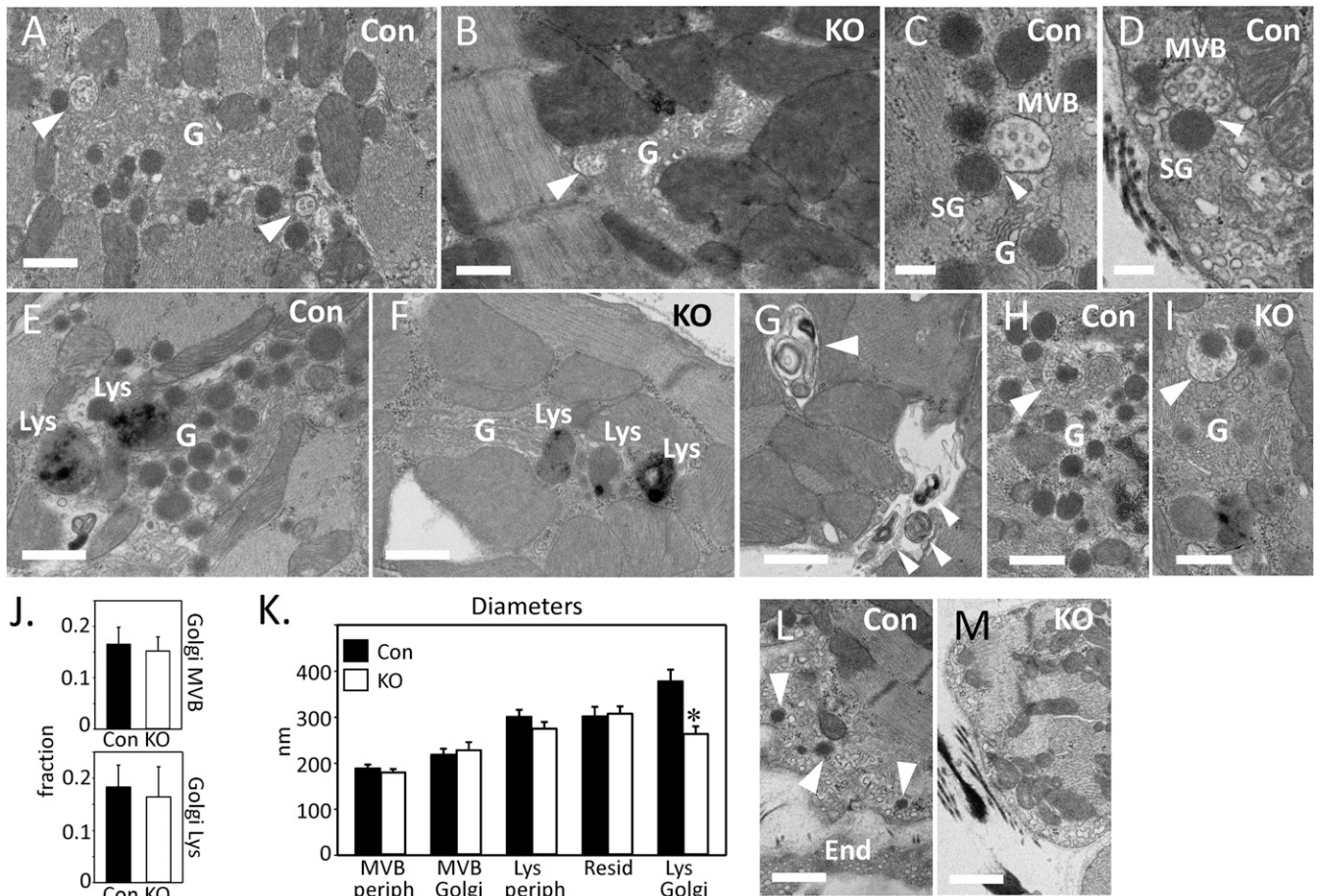

Fig. 2. Golgi-localized lysosomes are smaller in $Pam^{\text{Myh6-cKO/cKO}}$ atria. MVBs (arrowheads) in the Golgi (G) region in control (Con) (*A*, *C*, and *D*) and $Pam^{\text{Myh6-cKO/cKO}}$ (*B*) atrial myocytes. In controls, MVBs interacted closely with SGs in the Golgi area (*A* and *C*) and in the periphery (*D*). Dark, amorphous lysosomes (Lys) were seen near the Golgi complex in control (*E*) and $Pam^{\text{Myh6-cKO/cKO}}$ (*F*) atrial myocytes. Residual bodies in a control myocyte are shown (*G*, small arrowheads). In both control (*H*) and $Pam^{\text{Myh6−cKO/cKO}}$ (*I*) atrial myocytes, SG destruction by crinophagy occurs (arrowheads). The number of MVBs and Lys (*J*) located in the Golgi region did not vary with genotype. (*K*) MVB, Lys, and residual body (Resid) diameters were measured for organelles located peripherally (periph) or near the Golgi complex; Golgi-localized Lys were smaller in $Pam^{\text{Myh6-cKO/cKO}}$ atrial myocytes than in control cells (**P* < 0.005). The peripheral rim of cytoplasm was occupied by an extensive array of vesicles, vacuoles, and invaginations in control and KO cells (*L* and *M*); in control cells, SGs (arrowheads) were regularly observed. End, endothelial cell. (Scale bars, *A*, *B*, *E–I*, *L*, and *M*, 500 nm; *C* and *D*, 200 nm.)

www.manaraa.com

Granule Cargo Protein Levels Are Reduced in *Pam*[Myh6-cKO/+] Atria and Further Reduced in *Pam*[Myh6-cKO/cKO] Atria. Eliminating the expression of *Pam* in atrial cardiomyocytes resulted in decreased levels of proANP in the atrium (3). To determine the effect of loss of a single copy of *Pam*, we quantified PAM and proANP protein in atria from control mice, heterozygous mice (*Pam*[Myh6-cKO/+]), and *Pam*[Myh6-cKO/cKO] mice (Fig. 3*A*). As observed in adult *Pam*^{+/−} mice, levels of intact PAM protein in the atria of *Pam*[Myh6-cKO/+] mice were less than half of control values (33). PAM protein was undetectable in the atria of *Pam*[Myh6-cKO/cKO] mice. Levels of proANP fell below control values in atria from *Pam*[Myh6-cKO/+] mice and fell further in atria from *Pam*[Myh6-cKO/cKO] mice (Fig. 3*A*).

In addition to proANP, atrial granules contain proBNP and carboxypeptidase E (CPE) (15). As observed for proANP, levels of proBNP protein fell in *Pam*[Myh6-cKO/+] atria and fell further in *Pam*[Myh6-cKO/cKO] atria (Fig. 3*A*). In contrast, levels of CPE, another soluble cargo protein, were unaltered in atria lacking *Pam*. Glut4 (Slc2a4), a glucose transporter that is rapidly moved to the sarcolemma in response to insulin and enters proANP-containing granules after endocytic removal (34), was also examined. Levels of Glut4 protein were unaltered in atria lacking *Pam* (Fig. 3*A*). To determine the specificity of the changes observed, expression of markers for different organelles were also evaluated; no changes occurred (*SI Appendix*, Fig. S2*A*). Levels of several of the cytosolic and membrane proteins previously identified as PAM interactors were also unchanged in atria lacking *Pam*, but Vamp4 levels were reduced (*SI Appendix*, Fig. S2*B*) (35, 36). The lack of PAM protein exerted a cargo-specific effect on soluble secretory pathway proteins identified in atrial granules.

Subcellular Fractionation Confirms Decrease in SGs in *Pam*[Myh6-cKO/cKO] Mouse Atrium. The cytoplasmic volume fraction occupied by SGs fell 20-fold in the atria of *Pam*[Myh6-cKO/cKO] mice while atrial proANP levels fell only 3-fold. To determine the fate of granule content proteins in *Pam*[Myh6-cKO/cKO] atria, existing methods were modified to allow simultaneous evaluation of multiple organelles (16, 37, 38). Homogenization and differential centrifugation conditions were optimized for recovery of PAM and proANP in particulate fractions, with Gapdh, but very little proANP, in the cytosol (Fig. 3*B*). Intact PAM and proANP were enriched in the P3 fraction, with lower levels of intact PAM in P4, the fraction expected to contain endosomes. We next compared subcellular fractions prepared from the atria of control and *Pam*[Myh6-cKO/cKO] mice (Fig. 3*C*). Except for the absence of a prominent 16-kDa band, the mass of proANP and proBNP, in the P3 fraction of *Pam*[Myh6-cKO/cKO] mice (Fig. 3*C*, arrows in top panel), Coomassie staining revealed few differences. Nuclear, mitochondrial, lysosomal, Golgi, and vesicular trafficking markers were similarly localized in both genotypes (Fig. 3*C*).

Sucrose density-gradient centrifugation was used to separate atrial granules from lighter membranous organelles (39) (Fig. 3*D*). Antisera to endoplasmic reticulum (ER), Golgi, and endosomal markers revealed similar profiles for P3 pellets from control and *Pam*[Myh6-cKO/cKO] atria (*SI Appendix*, Fig. S3), with no clear separation of ER and Golgi markers. In P3 pellets from control atria, proANP was localized to the ER/Golgi region and to denser regions of the gradient, consistent with its presence in granules (Fig. 3*D*). The denser fractions accounted for 35.4 ± 2.5% of the total P3 proANP signal in control atria ($n = 4$), but only 25.7 ± 2.5% in *Pam*[Myh6-cKO/cKO] atria ($n = 2$; $P < 0.005$). The prominent
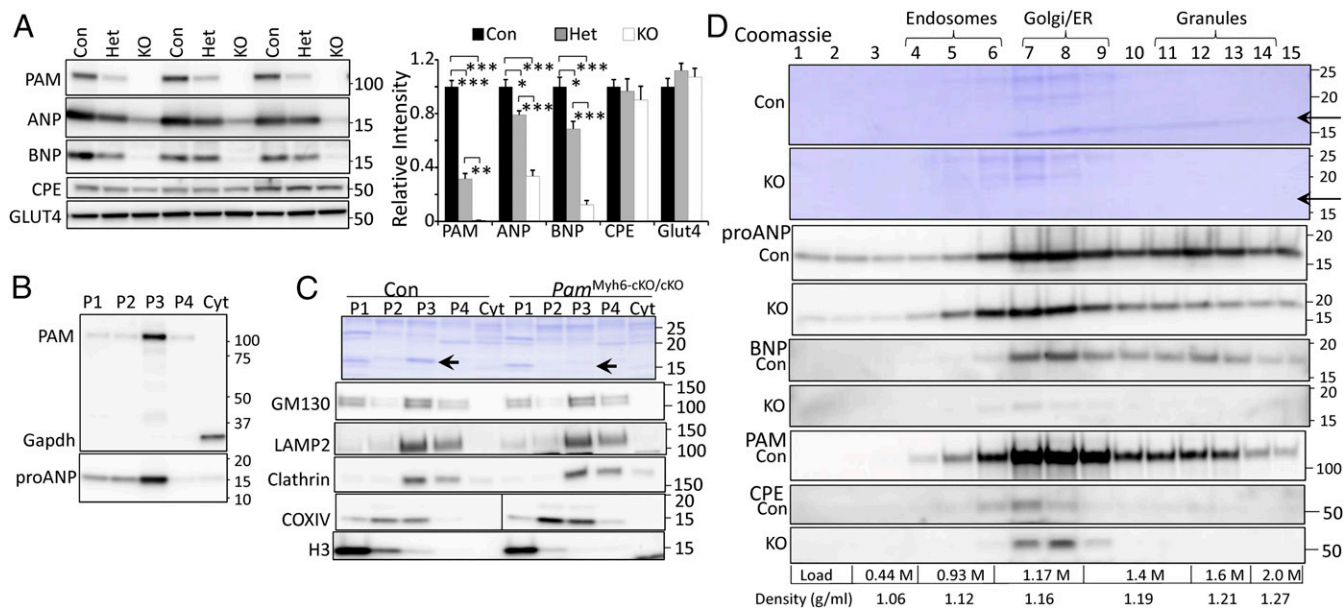

Fig. 3. PAM exerts a dosage-dependent, cargo-specific effect on atrial granules identified by subcellular fractionation. (*A*) Atrial lysates (20 μg) prepared from control (Con), heterozygous (Het, *Pam*[Myh6-cKO/+]), and homozygous (KO, *Pam*[Myh6-cKO/cKO]) adult male and female mice were fractionated by SDS/PAGE. Expression of PAM, three soluble secretory pathway cargo proteins (ANP, BNP, and CPE) and one membrane protein (GLUT4) were evaluated; *$P < 0.01$; **$P < 0.001$, ***$P < 0.0001$. (*B*) Western blot analysis was used to determine the localization of PAM, Gapdh, and proANP in subcellular fractions prepared from control adult male atria by differential centrifugation. (*C*) Subcellular fractions (equal amounts of protein) from control and *Pam*[Myh6-cKO/cKO] atria were fractionated by SDS/PAGE. The bottom part of the Coomassie-stained PVDF membrane is shown, with arrows marking a 16-kDa band seen only in control atria. Western blot analysis identified fractions enriched in Golgi membranes (GM130, 130-kDa *cis*-Golgi matrix protein), lysosomes (LAMP2, lysosome-associated membrane protein 2), trafficking vesicles (clathrin), mitochondria (COX IV), and nuclei (Histone H3, H3). (*D*) Sucrose density-gradient fractionation of P3 fractions from control and *Pam*[Myh6-cKO/cKO] (KO) atria. The bottom part of the Coomassie-stained PVDF membranes is shown, with arrows marking the Coomassie-stained 16-kDa band in control atria. The molarities and densities of the sucrose solutions used to form the step gradient appear at the bottom. Western blot analyses for proANP, BNP, and CPE from Con and KO atria are shown. PAM was detected in the ER/Golgi and granule-rich regions of the control gradient; 20.6 ± 0.7% ($n = 3$) of the PAM protein on the P3 gradient was recovered from the granule-rich region. Similar results were obtained in two additional direct comparisons of WT and *Pam*[Myh6-cKO/cKO] P3 fractions and in multiple analyses of WT P3 samples.

CELL BIOLOGY

Bäck et al.

www.manaraa.com

16-kDa Coomassie-stained band present in the control P3 fraction was distributed in a similar manner (Fig. 3D, arrows), with the granule region accounting for $33.9 \pm 4.7\%$ ($n = 3$) of the total 16-kDa Coomassie signal. As for proANP, Western blot analysis revealed peaks of proBNP in both the ER/Golgi and granule-enriched regions of the P3 gradient (Fig. 3D). In P3 fractions prepared from $Pam^{\text{Myh6-cKO/cKO}}$ atria, proBNP was detected in the ER/Golgi region, but not in the denser region.

To evaluate the specificity of this effect, the subcellular localization of CPE was determined. Unlike the natriuretic peptides, CPE was enriched in the ER/Golgi region, but not in the dense fractions, of control and $Pam^{\text{Myh6-cKO/cKO}}$ atria (Fig. 3D). Based on both transmission electron microscopy and biochemical fractionation, atrial myocyte PAM is essential for normal proANP and proBNP storage. With an almost complete loss of morphologically identifiable granules in $Pam^{\text{Myh6-cKO/cKO}}$ atria, proANP must occupy a different part of the secretory pathway.

Expression of PAM in $Pam^{\text{Myh6-cKO/cKO}}$ Atrial Myocytes Produces a Dose-Dependent, Activity-Independent Increase in proANP Levels.

Expression of PAM in rodent cardiomyocytes is readily detectable after embryonic day 14 (40). In order to determine whether the absence of atrial granules in adult $Pam^{\text{Myh6-cKO/cKO}}$ mice reflected a developmental defect, we prepared primary cultures from the atria of mice expressing two copies of the floxed Pam allele but no Cre-recombinase ($Pam^{0-Cre-\text{cKO/cKO}}$), meaning that PAM protein levels were normal. These atrial cultures were transduced with lentiviruses expressing GFP (control) or Cre-GFP (Fig. 4 A and B). After Cre-GFP-mediated excision of Pam exons 2+3, the decline in PAM protein reflects both the half-life of its mRNA and the half-life of the PAM protein. Levels of PAM, proANP, and Gapdh were unaltered in cultures expressing virally encoded GFP. In cultures expressing Cre-GFP, levels of PAM declined over time. As expected, levels of proANP fell more slowly, dropping about fourfold in 9 d (Fig. 4B). The time course over which proANP levels declined indicated that the ability of atrial myocytes to store proANP was dependent on the continued presence of PAM.

We next wanted to determine whether expression of exogenous PAM in atrial myocytes lacking any PAM could rescue proANP levels to those in control myocytes. To test this hypothesis, lentiviruses encoding rat PAM1 and rat PAM1/Met314Ile, a catalytically inactive mutant in which the monooxygenase active site methionine residue was replaced by isoleucine, were constructed (41) and validated by expression in HEK293 cells (*SI Appendix*, Fig. S4).

To evaluate the effect of expressing exogenous PAM1 or PAM1/Met314Ile on single myocytes, cultures were fixed and stained for proANP and for PAM. To validate our methodology, we first compared the properties of atrial myocytes prepared from control ($Pam^{0-Cre-\text{cKO/cKO}}$) and $Pam^{\text{Myh6-cKO/cKO}}$ (KO) mice (Fig. 4C); based on the developmental stage at which the Myh6 promoter becomes active and the time at which PAM is first expressed in the rodent atrium, PAM expression should never be initiated in $Pam^{\text{Myh6-cKO/cKO}}$ atrial myocytes (42). Using images captured under identical conditions, individual myocytes were evaluated for their content of PAM and proANP. In control myocytes, levels of both proANP and PAM in individual myocytes varied widely (Fig. 4D, black circles), as observed for several endocrine cell markers in single pancreatic β-cells (43). Quantification of both signals revealed a positive correlation ($R^2 = 0.54$); atrial myocytes with higher levels of PAM staining generally had higher levels of proANP staining. In $Pam^{\text{Myh6-cKO/cKO}}$ atrial myocytes, PAM staining was undetectable, but proANP levels again varied widely (Fig. 4D, gray boxes).

Atrial myocytes prepared from postnatal day 4 $Pam^{\text{Myh6-cKO/cKO}}$ pups were transduced with lentiviruses encoding PAM1 or PAM1/Met314Ile at the time of plating and examined 7 d later (Fig. 4C). PAM and proANP staining intensities were quantified in $Pam^{\text{Myh6-cKO/cKO}}$ cells expressing PAM1 or PAM1/Met314Ile (Fig. 4E). Strikingly, as levels of PAM1 expression rose, levels of proANP staining generally rose; the slope of this regression line was not as steep as the slope observed in control cells (Fig. 4D), but levels of proANP and PAM were highly correlated ($R^2 = 0.51$) (Fig. 4E, blue squares). There was a wide

Fig. 4. PAM expression increases proANP storage by $Pam^{\text{Myh6-cko/cko}}$ myocytes in a monooxygenase-activity independent manner. (A) Atrial cultures prepared from $Pam^{\text{cKO/cKO}}$ pups were spinoculated with virus encoding GFP or Cre-GFP. After 3, 6, or 9 d, cultures were harvested and equal amounts of cell protein (2.5 µg) were fractionated by SDS/PAGE; Western blot analysis for PAM (exon A antibody), Gapdh, and proANP revealed loss of PAM and proANP in cultures spinoculated with the Cre-GFP virus. (B) Immunoblot signals were densitized, with PAM and proANP levels normalized to Gapdh; data were normalized to levels on the first harvest day. The experiment was repeated with similar results. (C) Cultures were prepared at the same time from control ($Pam^{\text{cKO/cKO}}$) and $Pam^{\text{Myh6-cKO/cKO}}$ (KO) pups; control cultures were not spinoculated. $Pam^{\text{Myh6-cKO/cKO}}$ cultures were analyzed without spinoculation (no virus) or after spinoculation with lentiviruses encoding PAM1 or PAM1/Met314Ile. Seven days later, cultures were fixed and stained simultaneously for ANP (goat ANP antibody; Alexa633 secondary, shown in red), PAM (rabbit exon A antibody; Alexa488 secondary, shown in green), and nuclei (Hoechst stain; blue). Cultures were photographed under identical conditions; the exposure time for each fluorophore was adjusted to avoid saturation. Myocytes expressing higher and lower levels of PAM are indicated by an "#" and an "*", respectively; myocytes with ANP but no PAM are marked by "&." (D) Control and KO. Integrated total intensities for PAM and ANP staining were determined using Fiji and a locally determined background measurement for each cell. A range of PAM and ANP staining intensities was observed in control cells, clustered around a best-fit linear relationship (black circles). Variable ANP staining intensities were also observed in $Pam^{\text{Myh6-cKO/cKO}}$ cells, but no PAM staining was detected (gray squares). The x and y axes are arbitrary linear scales for reporting integrated total intensity per cell. The average integrated ANP staining intensity/cell in control atrial myocytes was cut in half in myocytes lacking PAM (2.77 ± 0.11 vs. 1.40 ± 0.08). (E) Rescue. Spinoculated cultures of $Pam^{\text{Myh6-cKO/cKO}}$ cells expressing PAM1 showed an increase in ANP staining intensity as PAM staining intensity increased (blue squares; blue line). A similar increase in ANP staining intensity was observed in $Pam^{\text{Myh6-cKO/cKO}}$ cells expressing PAM1/Met314Ile (M314I, orange diamonds; orange line). For comparison, the black line shows the least-squares best-fit line for Control cultures (dotted line in D).

Bäck et al.

www.manaraa.com
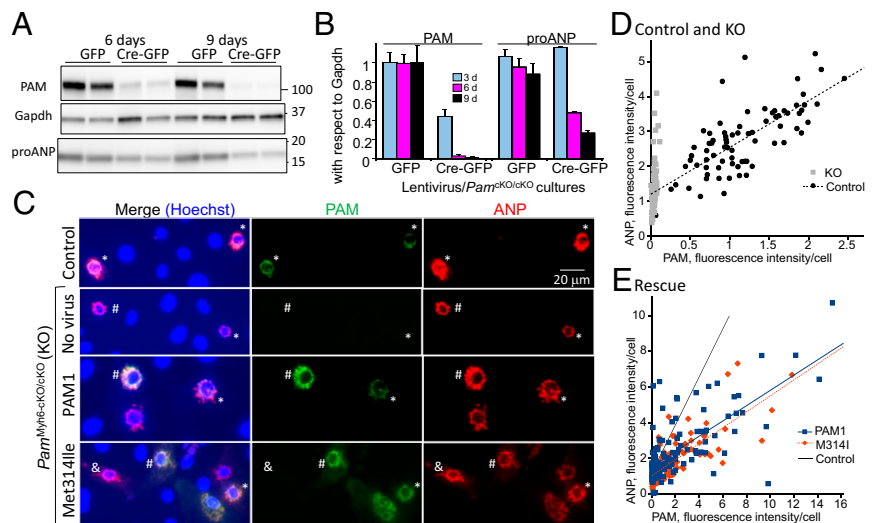
range of expression of PAM from the lentivirus, as expected from similar studies with isolated β-cells and virus-activated GFP expression (44). Analyses using a different pair of antibodies gave similar results (*SI Appendix*, Fig. S5). The ability of $Pam^{\text{Myh6-cKO/cKO}}$ atrial myocytes to store proANP was partially restored by expression of PAM.

Strikingly, in $Pam^{\text{Myh6-cKO/cKO}}$ myocytes expressing PAM1/Met314Ile, a similar correlation of proANP and PAM expression was observed (Fig. 4*E*, orange diamonds) ($R^2 = 0.60$). Based on this metric, the effects of PAM1 and PAM1/Met314Ile on the ability of atrial myocytes to store proANP were indistinguishable. Although the ability of PAM1 to increase proANP storage in atrial myocytes required high levels of PAM expression, it did not depend on its monooxygenase activity.

Basal Secretion and Turnover of proANP Are Increased in $Pam^{\text{Myh6-cKO/cKO}}$ Atrial Myocytes.

With a rise in *Nppa* transcript levels in $Pam^{\text{Myh-cKO/cKO}}$ atria (3), a decrease in the synthesis of proANP or an increase in its degradation or secretion could contribute to the threefold decline in proANP levels in the adult atrium. Metabolic labeling was used to compare the ability of control and $Pam^{\text{Myh-cKO/cKO}}$ atria to synthesize proANP (Fig. 5*A*). Total cell lysates and proANP immunoprecipitates were fractionated by SDS/PAGE and newly synthesized proANP was quantified by fluorography (*SI Appendix*, Fig. S6 *A* and *B*). No significant change in proANP synthesis was observed in $Pam^{\text{Myh-cKO/cKO}}$ atria when compared to control atria (Fig. 5*A*). To assess the possibility that the absence of PAM might trigger ER stress, resulting in proANP degradation, we evaluated several stress responsive cardiomyocyte proteins and transcripts (*SI Appendix*, Fig. S7 and Dataset S1 A and B) (45–47). The absence of PAM did not cause generalized ER stress or induce ER-phagy.

We next used cycloheximide to inhibit protein synthesis and determine the effect of genotype on the half-life of proANP. A genotype-specific difference in the stability of proANP was apparent by 2 h (Fig. 5*B*). The half-life of proANP in $Pam^{\text{Myh6-cKO/cKO}}$ myocytes across four experiments (5.5 ± 0.9 h) was approximately half that of proANP in control myocytes (11.7 ± 1.3 h) (*SI Appendix*, Fig. S6*C*). For comparison, the half-life of PAM in control myocytes

was 7.8 ± 1.1 h (*SI Appendix*, Fig. S6*D*). As expected, the half-life of Gapdh in both control and KO cultures was substantially greater than 30 h (*SI Appendix*, Fig. S6*D*) (48).

The decreased half-life of proANP in $Pam^{\text{Myh6-cKO/cKO}}$ myocytes could reflect an increase in secretion and in degradation. When maintained under the culture conditions used, cardiomyocytes secrete primarily intact proANP (49, 50), with little cleavage by Corin (4). To quantify secretion under the same basal conditions, cultures were incubated in complete serum-free medium. ProANP levels in cell lysates and media collected after 2 h were evaluated by Western blot and secretion, which was linear in time, was expressed as percent cell content released per hour (Fig. 5*C*). While control myocytes released $1.0 \pm 0.1\%$ of their proANP content per hour, $Pam^{\text{Myh6-cKO/cKO}}$ myocytes released $3.1 \pm 0.3\%$ of their proANP content per hour (Fig. 5*C*). This increase in proANP basal secretion would contribute to its decreased half-life in $Pam^{\text{Myh6-cKO/cKO}}$ myocyte cell extracts. The decreased levels of mature ANP observed in the sera of $Pam^{\text{Myh6-cKO/cKO}}$ mice may reflect a lack of proANP cleavage (3).

To determine whether increased degradation of proANP also contributed to its more rapid disappearance from $Pam^{\text{Myh6-cKO/cKO}}$ myocytes, cultures of both genotypes were treated with methylamine/ammonium chloride to raise luminal pH and inhibit lysosomal degradation, with MG132 or Bortezomib to inhibit proteasomal degradation, or with E-64 to inhibit calpain cleavage (Fig. 5*D*) (51). None of these treatments increased the proANP content of control or $Pam^{\text{Myh6-cKO/cKO}}$ atrial myocytes. Instead, MG132 reduced the proANP content of $Pam^{\text{Myh6-cKO/cKO}}$ atrial myocytes and Bortezomib reduced the proANP content of both control and $Pam^{\text{Myh6-cKO/cKO}}$ atrial myocytes. While our ultrastructural studies provided no evidence for an increase in lysosomes in $Pam^{\text{Myh6-cKO/cKO}}$ vs. control atria (Fig. 2*K*) and the protease inhibitors tested provided no support for increased proANP degradation in $Pam^{\text{Myh6-cKO/cKO}}$ myocytes, it is clear that more studies are needed to understand the effects of MG132, Bortezomib and E-64 on proANP levels in atrial myocytes.

Fig. 5. In the absence of PAM, the half-life of proANP is decreased and its basal secretion is increased. (*A*) Biosynthesis. Adult atrial tissue fragments (control and $Pam^{\text{Myh6-cKO/cKO}}$) were incubated in medium containing [^{35}S]Met/[^{35}S]Cys for 15 min. RIPA soluble protein (Lysate) and proANP immuno-precipitates (IPT) were fractionated by SDS/PAGE and newly synthesized proANP was quantified by fluorography; proANP is the major 16-kDa protein in atrial extracts (15), allowing its direct quantification (*SI Appendix*, Fig. S6 *A* and *B*). (*B*) Half-life. The half-lives of proANP, PAM, and Gapdh were determined using primary cultures of control and $Pam^{\text{Myh6-cKO/cKO}}$ atrial myocytes. A representative experiment using duplicate cultures incubated in medium containing 10 μM cycloheximide (CHI) for the indicated periods of time and analyzed as described in *Methods* is shown. Time-course data for proANP from this single experiment are plotted (*Right*); data for proANP, PAM, and Gapdh from four separate experiments are shown in *SI Appendix*, Fig. S6 *C* and *D*. (*C*) Basal secretion rate. Myocytes prepared from control and $Pam^{\text{Myh6-cKO/cKO}}$ pups were incubated in complete serum-free medium for 2 h; proANP levels in cell lysates and spent media were determined; basal secretion rates are expressed as percent cell content secreted per hour. (*D*) Protease inhibitors. Cultures treated with methylamine/NH$_4$Cl (MA/AC) for 2 to 12 h, MG-132 (MG) for 2 to 5 h, Bortezomib (Bort) or E-64 for 2 h were extracted for SDS/PAGE analysis of proANP levels; for each genotype, inhibitor-treated lysates were compared to corresponding control lysates. For *C* and *D*, *P* values in red report a genotype-specific effect of a drug (*t* test, control vs. KO) and *P* values in black report the effect of a specific drug on cultures of the indicated genotype (*t* test, no drug vs. drug).

Bäck et al.

www.manaraa.com
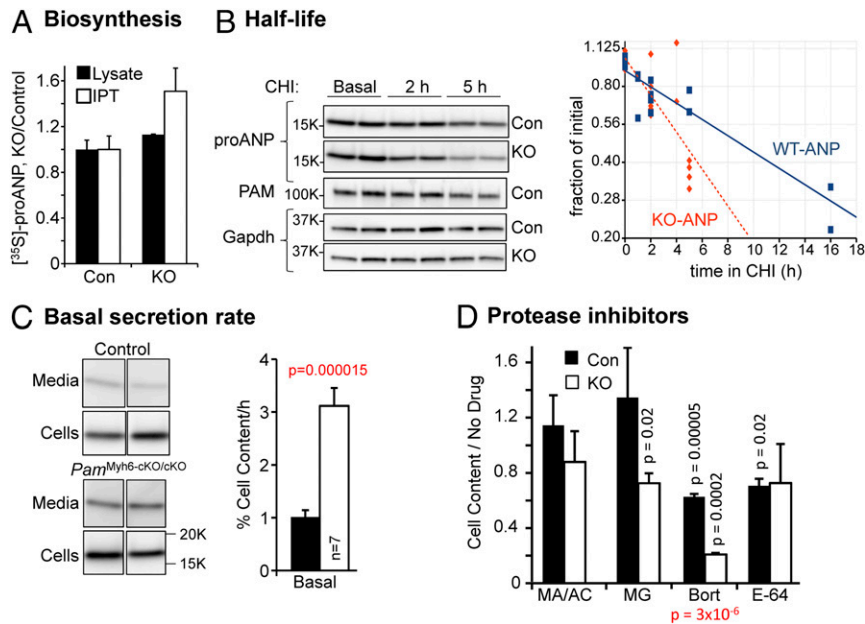
Exposure to BFA or Golgicide A Increased proANP Secretion by Control Myocytes but Not by $Pam^{Myh6-cKO/cKO}$ Myocytes. We employed several well-characterized pharmacological tools to explore the mechanism underlying the increased basal rate at which proANP is secreted by $Pam^{Myh6-cKO/cKO}$ atrial myocytes. Based on the literature, most of the proANP released basally by control atrial myocytes is newly synthesized (13, 52, 53). Consistent with these earlier studies, cycloheximide treatment reduced basal proANP secretion by control atrial myocytes to $42 \pm 13\%$ of the solvent control (Fig. 6 A and B). Cycloheximide had a smaller effect on the elevated basal secretion of proANP by $Pam^{Myh6-cKO/cKO}$ myocytes, reducing it to $63 \pm 9\%$ of the solvent control (Fig. 6 A and B) ($n = 9$, $P = 0.0002$) and suggesting a greater contribution of older proANP to basal secretion in atrial myocytes lacking PAM. The effects of cycloheximide on cell content of proANP over the course of this 2-h incubation were consistent with the half-lives reported in Fig. 5B, with a significant decline detectable in $Pam^{Myh6-cKO/cKO}$ myocytes but not in control myocytes (Fig. 6C).

The movement of cargo proteins from their site of synthesis in the ER through the Golgi complex and into SGs involves vesicular trafficking controlled by several Arf family small GTP binding proteins. Although BFA inhibits aspects of the basal and constitutive-like secretion of insulin, gastrin, and ACTH (8, 9) (*SI Appendix*, Fig. S8), it has been reported to stimulate the basal secretion of proANP by the intact adult rat atrium and by primary cultures of neonatal rat atrial myocytes (13, 14). In agreement with these studies, BFA produced a 2.5 ± 0.4-fold increase in proANP secretion by control mouse atrial myocytes (Fig. 6 A and B) ($n = 11$, $P = 0.0014$). Strikingly, BFA had no effect on the already elevated rate at which basal secretion of proANP occurred in $Pam^{Myh6-cKO/cKO}$ myocytes (Fig. 6 A and B) ($n = 9$, $P = 0.21$). Cell content of proANP was not affected by a 2-h BFA treatment in cultures of either genotype (Fig. 6C).

Golgicide A inhibits the activity of Golgi-specific BFA resistance GEF 1 (GBF1), the Arf GEF localized to the *cis*-Golgi area, without affecting the activity of BFA-inhibited GEF1 (BIG1) or BFA-inhibited GEF2 (BIG2), the Arf GEFs localized to later parts of the secretory pathway (10, 11). The actions of Golgicide A on basal proANP secretion mimicked those of BFA, with increased proANP secretion by control myocytes and no effect on $Pam^{Myh6-cKO/cKO}$ myocytes (Fig. 6 A and B). Corticotrope tumor cells were used to verify the ability of BFA and Golgicide A to inhibit specific aspects of the basal, constitutive-like and regulated secretion of prohormone convertase 1 and POMC products (*SI Appendix*, Fig. S8). The fact that basal proANP secretion by atrial myocytes lacking PAM resembled proANP secretion by Golgicide A-treated control myocytes suggested that inhibition of GBF1 prevented PAM from carrying out its normal role in the secretion of proANP by atrial myocytes, and that PAM affected proANP handling early in the secretory pathway.
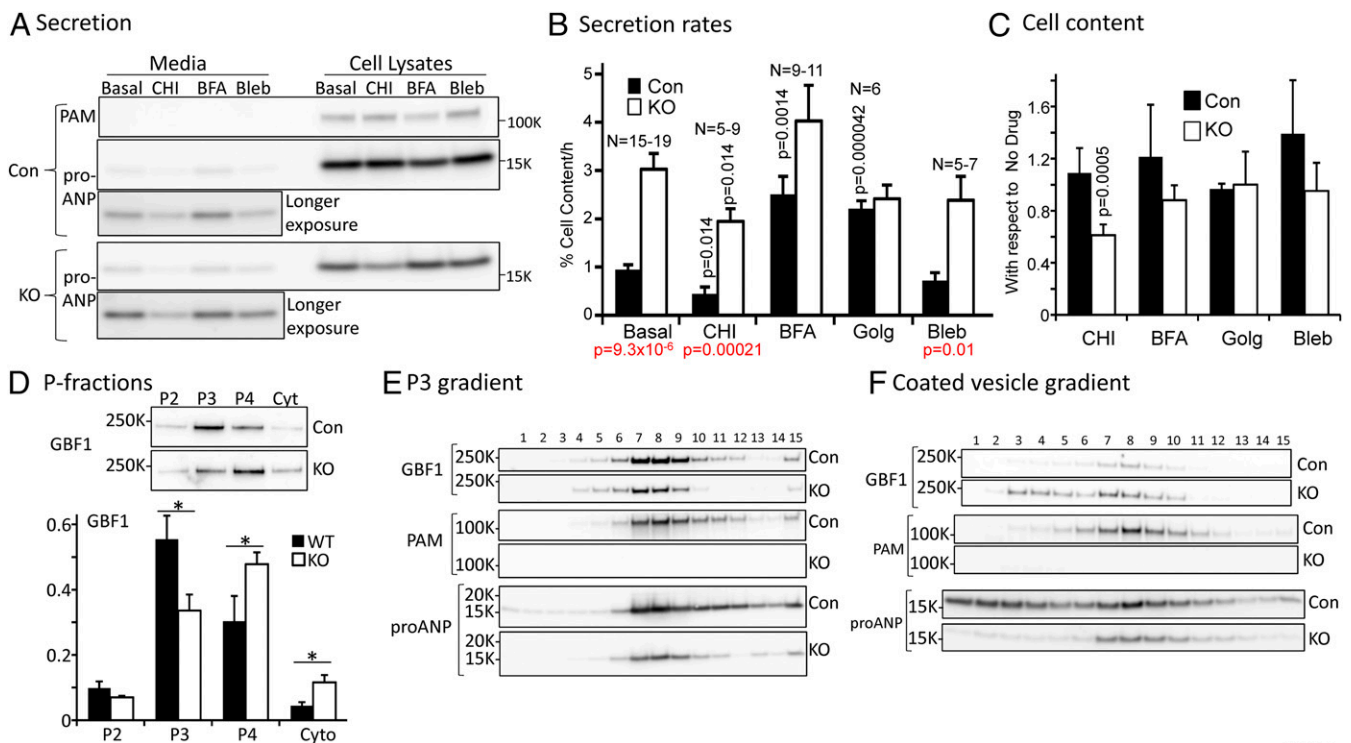

Fig. 6. PAM affects proANP trafficking through early parts of the secretory pathway. (*A*) Secretion and (*B*) secretion rates. The effects of cycloheximide (CHI, 10 μM, with a 1-h pretreatment), BFA (7.1 μM), Golgicide A (Golg, 10 μM), and blebbistatin (Bleb, 10 μM) on the secretion of proANP by control (Con) and $Pam^{Myh6-cKO/cKO}$ (KO) myocytes were determined. In the example shown, the litter used to prepare cultures contained one Con and five KO pups; media and cell extracts were analyzed simultaneously. Secretion rates are expressed as percent proANP cell content released per hour; *n* values for each comparison are shown. Statistics (*t* test): *P* values for drug vs. control of the same genotype are shown in black and *P* values for genotype-specific drug effects are shown in red. (*C*) Cell content. Drug effects on cell content of proANP (proANP/Gapdh) in control and KO cultures are shown. (*D*) P-fractions. As described for Fig. 3*C*, subcellular fractions prepared from Control and $Pam^{Myh6-cKO/cKO}$ atria were analyzed for their content of GBF1; a genotype-specific difference was observed ($P = 0.0039$, two-way ANOVA; $*P < 0.05$ for post-hoc pairwise *t* test). (*E*) P3 gradient. P3 fractions prepared from Control and $Pam^{Myh6-cKO/cKO}$ atria were subjected to sucrose gradient fractionation; immunoblot analyses were used to localize GBF1, PAM, and proANP. The entire experiment was repeated, with similar results. (*F*) Coated vesicle gradient. Coated vesicles prepared simultaneously from Con and $Pam^{Myh6-cKO/cKO}$ atria were subjected to sucrose gradient fractionation. Expression of GBF1, PAM, and proANP was evaluated in aliquots representing equal amounts of input protein. The entire experiment was repeated, with similar results.

www.manaraa.com

Blebbistatin, a myosin II-specific inhibitor (54), blocks tropomyosin 4.2-dependent ER to Golgi trafficking in mouse embryonic fibroblasts (55) and BFA-induced retrograde *cis*-Golgi to ER trafficking in pheochromocytoma cells (56). Blebbistatin had no effect on the rate at which proANP was secreted by either control or *Pam*^Myh6-cKO/cKO myocytes (Fig. 6 *A* and *B*).

GBF1 Localization Is Altered in *Pam*^Myh6-cKO/cKO Atrial Myocytes. To explore the mechanism through which Golgicide A increases proANP secretion by control, but not by *Pam*^Myh6-cKO/cKO myocytes, we examined GBF1 expression and subcellular localization in atria of both genotypes; GBF1 is expressed at similar levels (10 to 20 reads per kilobase per million mapped reads) in most adult mouse tissues (National Center for Biotechnology Information gene 107338). Levels of GBF1 protein did not differ in control and *Pam*^Myh6-cKO/cKO atria (*SI Appendix*, Fig. S9 *A* and *B*), but differential centrifugation revealed a shift in its localization (Fig. 6*D*). In control tissue, GBF1 was most enriched in the P3-fraction, with much lower levels in the cytosol. In P-fractions prepared from *Pam*^Myh6-cKO/cKO atria, enrichment of GBF1 in the P3-fraction fell, while enrichment in the P4- and cytosolic fractions rose.

Sucrose density-gradient fractionation of P3-fractions from control atria revealed remarkable similarities in the localization of GBF1 and PAM; both proteins were present in the denser regions of the gradient (fractions 11 to 14), along with proANP (Fig. 6*E*). As observed for proANP, less of the GBF1 was recovered from the dense region of sucrose density gradients prepared from P3-fractions of *Pam*^Myh6-cKO/cKO atria.

Analysis of *Pam*^+/− mice and rescue experiments revealed that atrial granule formation required high levels of PAM. Evidence for a direct interaction of PAM with proANP comes from the expression of fluorescently tagged PAM in cardiomyocytes (18), suggesting that PAM might act as a chaperone or transporter, facilitating proANP entry into granules. The ability of catalytically inactive PAM to restore proANP storage supports this hypothesis (Fig. 4 and *SI Appendix*, Fig. S5). Molar levels of proANP, which accounts for over 95% of the soluble protein in atrial granules, would be expected to greatly exceed molar levels of PAM and the recycling of PAM would be required for normal granule biogenesis (16, 52). Depletion or inhibition of GBF1 is known to block the recruitment of COPI coats to membranes of the *cis*-Golgi (10). If inhibiting GBF1 with Golgicide A blocked the return of PAM from the *cis*-Golgi or immature atrial granules to the ER, proANP traversing the control cell secretory pathway might be susceptible to basal release, as in *Pam*^Myh6-cKO/cKO myocytes.

To test this hypothesis, we assessed the localization of GBF1, PAM, and proANP in coated vesicles prepared from control and *Pam*^Myh6-cKO/cKO adult mouse atria (Fig. 6*F*). Consistent with the increased amount of GBF1 recovered from the P4-fraction of *Pam*^Myh6-cKO/cKO atria, a stronger GBF1 signal was observed in coated vesicles prepared from these atria. Levels of the mRNAs encoding GBF1, the Arf proteins, and the coatomer subunits did not differ in control and *Pam*^Myh6-cKO/cKO atria (Dataset S1C). As for GBF1, levels of GM130, ER-Golgi intermediate compartment, 53-kDa protein (ERGIC-53), Sec13, and Sar1B protein (*SI Appendix*, Fig. S9 *A* and *B*) did not differ in control and *Pam*^Myh6-cKO/cKO atria. Based on marker protein localization, coated vesicles were enriched in gradient fractions 8 to 12 (*SI Appendix*, Fig. S9C); negative staining confirmed the presence of structures of the right size to be coated vesicles (*SI Appendix*, Fig. S9D).

While COPII-coated vesicles would be expected to contain newly synthesized PAM and newly synthesized proANP, COPI-coated vesicles would be expected to carry PAM being recycled to the ER. With the small amounts of material available, we did not attempt to separate COPI- and COPII-coated vesicles. Instead, we searched for a genotype-specific difference in protein localization (Fig. 6*F*). In control atria, PAM and GBF1 were

similarly localized (Fig. 6*F*). The localization of GBF1 in coated vesicles prepared from *Pam*^Myh6-cKO/cKO atria differed, with an additional peak at lower density; this difference in GBF1 localization supports the hypothesis that PAM affects Golgi/ER vesicular trafficking. ProANP was recovered from the coated vesicle-enriched fractions of both control and *Pam*^Myh6-cKO/cKO atria (Fig. 6*F*); proANP recovered from the low-density region of control samples may reflect atrial granule disruption by the sonication step used to prepare coated vesicles.

PAM Facilitates proANP Storage in Atrial Granules by Altering Its Pre-Golgi Trafficking. We used HEK293 cells, which lack secretory granules and any of the features unique to cardiomyocytes, to test the hypothesis that PAM alters the trafficking of proANP at an early stage in the secretory pathway. Since the synthesis of proANP requires intrachain disulfide bond formation, but not N-glycosylation, endoproteolytic cleavage, or extensive O-glycosylation (57), its synthesis in HEK293 cells should proceed without difficulty. ProANP-Emerald (58, 59) was transiently expressed in HEK293 cells and in HEK293 cells stably expressing PAM1 (PAM/HEK) at levels similar to those observed in the adult mouse atrium (*SI Appendix*, Fig. S10A). proNPY-GFP (60), another soluble protein efficiently targeted to secretory granules in neuroendocrine cells, was also transiently expressed in HEK293 and PAM/HEK cells (*SI Appendix*, Fig. S10 *B* and *C*).

When expressed in HEK293 cells, both proANP-Emerald and proNPY-GFP were generally diffusely distributed (Fig. 7*A*). In contrast, when expressed in PAM/HEK cells, proANP-Emerald was often condensed in the perinuclear region (Fig. 7*A*). In cells expressing lower levels of proANP-Emerald, a more diffuse accumulation was observed in the perinuclear region (Fig. 7*A*). The localization of transiently expressed proNPY-GFP was also affected by the presence of PAM, but condensation in the perinuclear region of PAM/HEK cells was rarely observed (Fig. 7*A*). To evaluate the localization of these transiently expressed proteins, epifluorescence images of HEK293 and PAM/HEK cells expressing proANP-Emerald or proNPY-GFP were categorized as diffuse, perinuclear, or condensed (Fig. 7*B*). The accumulation of bright, punctate structures near the nucleus (the condensed phenotype) was largely limited to cells expressing PAM and proANP-Emerald (Fig. 7*B*).

Confocal images of PAM/HEK cells expressing proANP-Emerald revealed extensive overlap of PAM and proANP-Emerald in reticular structures and in puncta (Fig. 7 *C*, *Inset 1*, yellow arrows). Small puncta containing proANP (Fig. 7 *C*, *Inset 1*, short green arrows), or PAM (Fig. 7 *C*, *Inset 1*, white arrows) were also seen. The localization of proANP and PAM was compared to that of ERGIC-53, a marker for ER exit sites (ERESs) and the tubulovesicular clusters responsible for the bidirectional traffic that connects the ER to the *cis*-Golgi (Fig. 7 *C*, *Insets 2* and *3*) (61, 62). ERGIC-53^+ puncta (Fig. 7 *C*, *Insets 2* and *3*, red arrows) were often localized adjacent to proANP-Emerald^+ and PAM^+ tubulovesicular structures (Fig. 7 *C*, *Insets 2* and *3*, respectively), but neither proANP-Emerald nor PAM accumulated in the ERGIC-53^+ puncta. Extensive overlap was observed when PAM/HEK cells expressing proANP-Emerald were stained for PAM and GM130 (Fig. 7*D*). Staining for PAM (Fig. 7 *D*, *Inset 1*, white arrows) and for GM130 (Fig. 7 *D*, *Inset 1*, red arrows) was frequently overlapping or immediately adjacent. Staining for proANP and GM130 (Fig. 7 *D*, *Inset 2*) was often coincident. Taken together, our data indicate that expression of PAM facilitates the accumulation of proANP in the *cis*-Golgi region and that proANP does not accumulate at ERESs.

Discussion

PAM Plays a Role in Basal proANP Secretion and Granule Formation. Eliminating *Pam* expression in atrial myocytes resulted in a 3-fold drop in proANP levels in the atrium, a 13-fold decline in
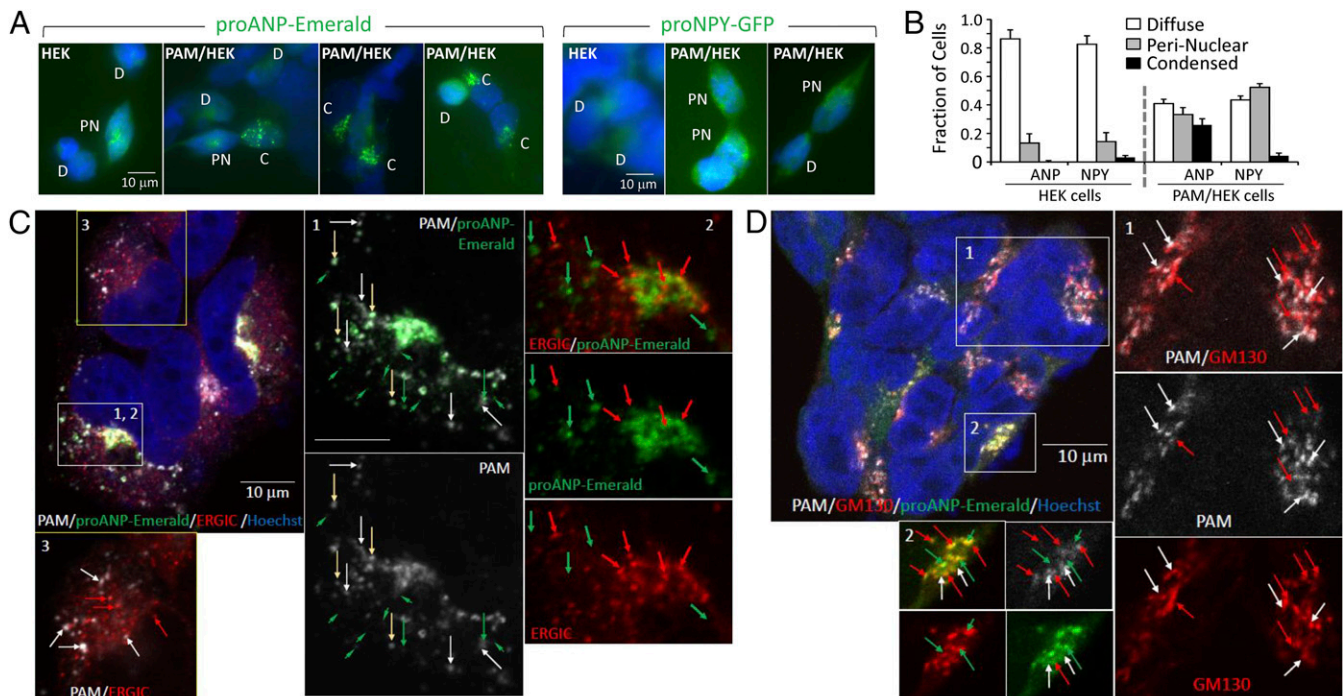
CELL BIOLOGY

Fig. 7. Expression of PAM in cells lacking secretory granules alters proANP trafficking. Sparsely plated HEK cells and PAM/HEK cells transiently transfected the previous day with vectors encoding proANP-Emerald or proNPY-GFP were fixed; nuclei were visualized using Hoechst stain and epifluorescence images of the transiently expressed proteins were collected using a 40× objective. Coverslips were scanned systematically and cells expressing a fluorescently tagged protein were imaged under standard conditions. Fluorescent protein localization was categorized as diffuse (D), perinuclear (PN), or condensed (C) by a blinded observer. (*A*) Examples illustrating the three staining categories are shown for proANP-Emerald and for proNPY-GFP expressed in HEK or PAM/HEK cells. (Scale bar, 10 μm for all images.) (*B*) Quantitative data for each cell type and vector are shown; the number of cells and number of groups averaged were HEK-ANP (236, 4), HEK-NPY (932, 7), PAM/HEK-ANP (514, 5), PAM/HEK-NPY (222, 5). Based on a two-way ANOVA, the behavior of the two cell lines and the two fluorescently tagged proteins differed ($P < 0.0001$ for all comparisons). (*C* and *D*) Confocal images were obtained for PAM/HEK cells expressing proANP-Emerald (green) and stained for PAM (gray) and ERGIC-53 (red) (*C*) or for PAM (gray) and GM130 (red) (*D*). Numbered insets are shown at higher magnification with single colors or two colors, as indicated; *C*1, 2.6-fold, *C*2, 2.5-fold, *C*3, *D* 1 and 2, 1.5-fold.

granule number per cell, and a 3-fold increase in proANP basal secretion rate. While the decrease in proANP levels can be accounted for in part by the increase in basal secretion, the almost complete absence of atrial granules suggested a specific role for PAM in granule formation or stability. PAM expression in the atrium exceeds levels in all other tissues; since the natriuretic peptides are not amidated, it was proposed that PAM facilitates their condensation and storage, as observed for secretogranins (15, 16). Our data establish a noncatalytic role for PAM in the atrium and localize its actions to early stages of the secretory pathway (Fig. 8).

Demonstration of a direct interaction between PAM and proANP will require additional experimentation, but multiple observations support the proposal. A conserved pair of adjacent acidic residues near the N terminus of proANP plays an essential role in its ability to bind Ca^{2+}, aggregate and enter the regulated secretory pathway (63). These same residues play an essential role in the ability of proANP to interact with PAM in transfected atrial myocytes (18, 58). PAM and proANP together account for 95% of the protein in atrial granule membranes (16) and the effects of PAM on proANP storage were dose-dependent and selective. Natriuretic peptide levels in the atria of mice with a single *Pam* allele were reduced, but not to the levels observed in *Pam*[Myh6-cKO/cKO] mice; CPE levels were unaltered. Expression of exogenous PAM increased proANP storage in *Pam*[Myh6-cKO/cKO] atrial myocytes in a dose-dependent manner that did not require its monooxygenase activity. When transiently expressed in cells that lack SGs and express PAM at low levels, proANP-Emerald was diffusely distributed; in lines stably expressing PAM at levels

observed in the atrium, proANP-Emerald and PAM were largely localized near GM130^{+}, perinuclear structures.

Taken together, these diverse observations support a working model built around a low-affinity, direct interaction between the luminal domains of PAM and proANP (Fig. 8). The model incorporates a direct interaction of PAM with newly synthesized proANP, facilitating proANP delivery to the *cis*-Golgi and to immature granules and preventing its basal secretion (Fig. 8). The ability of Golgicide A, a specific inhibitor of GBF1, the Arf-GEF localized to the *cis*-Golgi, to stimulate proANP secretion by control atrial myocytes without affecting proANP secretion by *Pam*[Myh6-cKO/cKO] atrial myocytes focused our attention on a mechanism through which PAM could limit basal proANP secretion. Studies on the roles of the luminal and cytosolic domains of PAM in its trafficking through the biosynthetic and endocytic compartments of corticotrope tumor cells guided our interpretation of its role in myocytes.

Basal Secretion of proANP. Studies using intact atria and primary rodent atrial myocyte cultures established the key features of basal proANP release. Unlike most peptide hormones and neuropeptides, much of the proANP secreted basally is recently synthesized (13, 53), suggesting that it might not have traversed the Golgi complex. While increased intracellular calcium stimulates the secretion of most peptide hormones and neuropeptides (8, 9) (*SI Appendix*, Fig. S8), it inhibits the basal secretion of natriuretic peptides (5, 6). Unlike the stimulated secretion of proANP, its basal secretion is not affected by pertussis toxin or by monensin. BFA treatment of
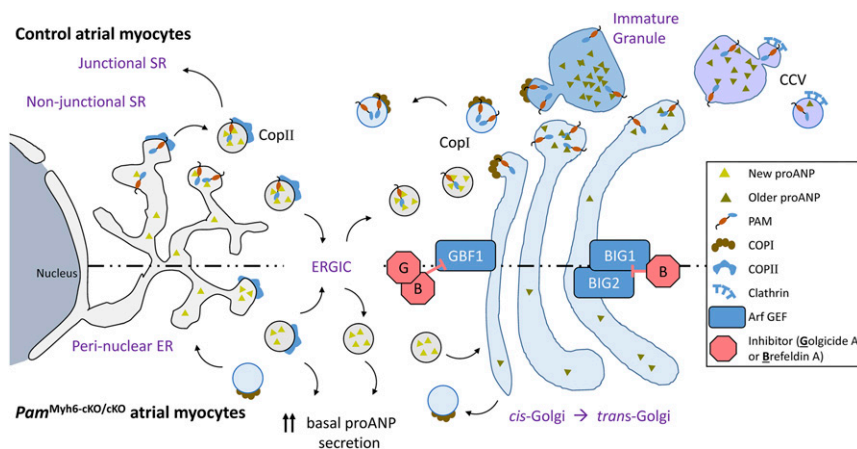
Bäck et al.

www.manaraa.com

Fig. 8. Working model. Key differences in the trafficking of newly synthesized proANP from its site of synthesis in the perinuclear ER through the ER/Golgi intermediate compartment (ERGIC) and into the *cis*-Golgi and immature secretory granules in Control (above the dashed line) and *Pam*^Myh6-cKO/cKO atrial myocytes are indicated. BIG1 and -2, BFA-inhibited GEF1 and -2; CCV, clathrin coated vesicle; CopI and II, COPI- and COPII-coated vesicles; GBF1, Golgi-specific BFA-resistance guanine nucleotide exchange factor 1; SR, sarcoplasmic reticulum.

cannulated atria or cultured atrial myocytes increases basal proANP release (13, 14). Using primary cardiomyocyte cultures, we confirmed the ability of BFA to increase basal proANP release and demonstrated the ability of Golgicide A to do the same. Based on these observations, basal proANP secretion does not require Arf-activated vesicular trafficking, suggesting that it comes largely from a source that precedes the *cis*-Golgi.

Unique features of the ER/SR in atrial myocytes may contribute to the unusual features of proANP secretion. Transverse tubules, which are prevalent in ventricular myocytes, are rare in atrial myocytes (64). Instead, junctional SR underlies the sarcolemma, connected to the perinuclear ER by nonjunctional SR. Calsequestrin, a soluble calcium-binding protein, moves from its site of synthesis in the perinuclear ER to the lumen of the junctional SR, where it plays a role in calcium release; this process is inhibited by disruption of COPII-mediated vesicular budding, but not by disruption of intra-Golgi trafficking (65). The machinery that allows calsequestrin to travel from its site of synthesis to the junctional SR could provide a pathway through which newly synthesized proANP is basally secreted without traversing the Golgi complex.

Some membrane proteins exit the ER in non-COPII vesicles or bypass the Golgi complex, yet still reach the plasma membrane (66). The cystic fibrosis transmembrane conductance regulator exits the ER in a COPII-dependent manner, but bypasses the Golgi complex, accumulating in a pericentriolar intermediate compartment (66). In neurons, a significant fraction of the forward trafficking from ER to dendritic recycling endosomes and the plasma membrane occurs even when the Golgi apparatus has been disrupted by BFA, and many surface receptors have immature N-linked glycans, consistent with Golgi bypass (61). A Golgi bypass pathway would allow production of proANP, which does not require N-glycosylation, is not extensively O-glycosylated, and is cleaved only at the time of secretion (57).

PAM Protects Newly Synthesized proANP from Basal Release and Delivers proANP to Nascent Granules. The exit of newly synthesized proteins from the ER involves bulk flow and active sorting. Soluble cargo proteins like proANP can enter COPII vesicles by diffusing into a budding zone, or can be concentrated in COPII vesicles through interactions with p24 family proteins or general cargo receptors like ERGIC-53, a lectin with COPII sorting signals (67). The cytosolic domain of PAM has highly conserved diacidic and dihydrophobic motifs resembling those that allow the vesicular stomatitis virus glycoprotein and ERGIC-53, respectively, to bind to COPII coat proteins (67). While the ER is a single continuous structure, different functions are carried out in

distinct zones. Cargo often exits the ER at ribosome-free subdomains (ERESs or transitional ER), where COPII coated vesicles are concentrated (67). In vertebrate cells, ERESs are distributed across the ER, with many far removed from the Golgi complex. The vesicular tubular clusters that comprise the ERGIC receive cargo from ER exit sites, and link it to the *cis*-Golgi (68) (Fig. 8).

The rate at which proANP was basally secreted by atrial myocytes lacking PAM was equal to the rate at which proANP was secreted by BFA-treated atrial myocytes expressing PAM, suggesting that PAM protected newly synthesized proANP from basal secretion. Although the pathway through which BFA stimulates the basal secretion of proANP has not been elucidated, the fact that it does so only in the presence of PAM suggested the involvement of altered PAM trafficking. The ability of Golgicide A to mimic this effect of BFA identified the *cis*-Golgi as the key site for this effect. With proANP levels exceeding PAM levels, PAM would need to be recycled to the ER after accompanying proANP to the *cis*-Golgi and perhaps to nascent secretory granules (Fig. 8). Blocking the return of PAM to the ER would leave newly synthesized proANP susceptible to secretion via an early BFA-insensitive pathway. A study of procathepsin secretion after its removal from immature secretory granules in β-cells revealed a stimulatory effect of BFA on its release from recycling endosomes (7).

There is a precedent for COPI-dependent return of cargo receptors to the ER. Yeast Erv29p and its *Caenorhabditis elegans* homolog, SFT-4/Surf4 (Surfeit locus protein 4 homolog), are ER-localized membrane proteins required for the efficient COPII-mediated export of specific soluble cargo proteins; these cargo receptors are returned to the ER in COPI-coated vesicles (69). TANGO1 (Transport and Golgi organization protein 1), a type 1 ER-localized membrane protein, delivers procollagen to departing COPII vesicles, but remains in the ER (67). Our data suggest that the actions of PAM resemble those of Erv29p and SFT-4.

The cytosolic domain of PAM interacts with the μ1A subunit of the AP-1 complex (70), with Rho GEFs that activate Rac1, RhoG, and RhoA (71), and with actin (72). In corticotrope tumor cells, PAM enters immature SGs, produces amidated products and is removed in an AP-1–dependent process. The ability of the cytosolic domain of PAM to interact with μ1A plays an essential role in granule maturation, and the endocytic trafficking of PAM is guided by the reversible phosphorylation of multiple Ser/Thr residues in its cytosolic domain. The μ1A subunit most closely resembles the δCOP subunit of COPI (73). PAM was identified in atrial coated vesicle-enriched fractions. Subcellular fractionation revealed remarkably similar

distributions for PAM and GBF1 during sucrose gradient fractionation of control P3 fractions, with altered GBF1 localization in *Pam*^Myh6-cKO/cKO P3 fractions. GBF1 and PAM were similarly localized following sucrose density-gradient fractionation of coated vesicles prepared from control tissue; GBF1 localization was again affected by the absence of PAM. The fact that PAM expressed in cells lacking SGs localized to the *cis*-Golgi region and altered the localization of transiently expressed proANP-Emerald is consistent with a role for PAM in the early secretory pathway, preceding the Golgi complex. The effects of PAM on soluble cargo trafficking are not limited to proANP. High levels of PAM expression in HEK cells led to proNPY accumulation in the perinuclear region. In AtT-20 corticotrope tumor cells, PAM expression leads to POMC accumulation in the *trans*-most cisternae of the Golgi complex, limiting its cleavage and storage of its product peptides in secretory granules (74).

Left atrial function is an independent predictor of adverse cardiac events in the general population and in hypertension and heart failure patients (75) and atrial failure, in the absence of ventricular or valvular abnormalities, can cause heart failure (76). The current understanding of protein trafficking, signaling, and cytoskeletal control in atrial myocytes is limited. In *Pam*^Myh6-cKO/cKO atrial myocytes, fewer Golgi complexes were found near the sarcolemma. Left atrial myocytes in tissue from atrial fibrillation patients exhibited Golgi fragmentation, with an increase in smaller fragments localized lateral to the nucleus (25). Understanding how rhythmic contraction, a known regulator of the atrial myocyte cytoskeleton (77), affects the protein trafficking network in which PAM and proANP function may reveal new ways in which to manipulate the system.

Methods

Detailed methods appear in *SI Appendix*.

Mouse Husbandry. PAM^cKO mice are available from The Jackson Laboratory as JAX#034076. All work with mice was approved by the University of Connecticut Health Center Institutional Animal Care and Use Committee.

Biochemical Analyses. SDS/PAGE and subcellular fractionation of atria from adult male and female C57Bl6/J, other control and *Pam*^Myh6-cKO/cKO mice were carried out using minor modifications of previously published procedures (16, 37, 38). For the preparation of atrial coated vesicles, methods used to process large amounts of tissue (78) were modified to handle the small amounts of atrial tissue available.

Transmission Electron Microscopy and Image Analysis. Fixed atria from adult *Pam*^cKO/cKO and *Pam*^Myh6-cKO/cKO mice were systematically photographed at fixed intervals with a random start. Morphometric analysis was performed with the Stereology function in Microscopy Image Browser (79).

Cell Culture. Control and *Pam*^Myh6-cKO/cKO cultures were prepared from the atria of genotyped, postnatal day 4 to 7 pups. Atrial myocytes plated at a density of ~1 atrium/well of a 96-well dish were maintained in medium that does not support proANP cleavage (49). For analysis of basal proANP secretion, cell extracts and media were fractionated at the same time, allowing calculation of secretion rates, which were linear with time (percent cell content secreted per hour). Lentiviruses encoding PAM1, PAM1/Met314Ile, GFP, and Cre-recombinase-GFP were obtained from the University of Iowa Viral Vector Core (University of Iowa Health Care, Iowa City, IA). Freshly dissociated atrial myocytes were spinoculated at the time of plating and analyzed up to 11 d later (80). HEK293 cells stably expressing rat PAM1 were transiently transfected with vectors encoding proANP-Emerald or proNPY-GFP using TransIT-2020 (Mirus Bio).

Statistical Analyses. Pairwise comparisons were performed using Student's *t* test (Excel or Open Office). ANOVAs were performed using GraphPad Prism 8. Linear best-fit lines were assigned using Open Office.

Data Availability. All data are available in the paper or in the *SI Appendix*. Antibodies, cell lines, and plasmids will be supplied promptly upon request by qualified researchers.

1. A. Matsuo, C. Nagai-Okatani, M. Nishigori, K. Kangawa, N. Minamino, Natriuretic peptides in human heart: Novel insight into their molecular forms, functions, and diagnostic use. *Peptides* **111**, 3–17 (2019).
2. M. F. McGrath, M. L. K. de Bold, A. J. de Bold, The endocrine function of the heart. *Trends Endocrinol. Metab.* **16**, 469–477 (2005).
3. K. G. Powers, X. M. Ma, B. A. Eipper, R. E. Mains, Identifying roles for peptidergic signaling in mice. *Proc. Natl. Acad. Sci. U.S.A.* **116**, 20169–20179 (2019).
4. W. Yan, F. Wu, J. Morser, Q. Wu, Corin, a transmembrane cardiac serine protease, acts as a pro-atrial natriuretic peptide-converting enzyme. *Proc. Natl. Acad. Sci. U.S.A.* **97**, 8525–8529 (2000).
5. M. F. McGrath, A. J. de Bold, Determinants of natriuretic peptide gene expression. *Peptides* **26**, 933–943 (2005).
6. J. E. Greenwald, M. Apkon, K. A. Hruska, P. Needleman, Stretch-induced atriopeptin secretion in the isolated rat myocyte and its negative modulation by calcium. *J. Clin. Invest.* **83**, 1061–1065 (1989).
7. M. D. Turner, P. Arvan, Protein traffic from the secretory pathway to the endosomal system in pancreatic beta-cells. *J. Biol. Chem.* **275**, 14025–14030 (2000).
8. X. F. Huang, P. Arvan, Formation of the insulin-containing secretory granule core occurs within immature beta-granules. *J. Biol. Chem.* **269**, 20838–20844 (1994).
9. A. Varro, J. Henry, C. Vaillant, G. J. Dockray, Discrimination between temperature- and brefeldin A-sensitive steps in the sulfation, phosphorylation, and cleavage of progastrin and its derivatives. *J. Biol. Chem.* **269**, 20764–20770 (1994).
10. F. Manolea, A. Claude, J. Chun, J. Rosas, P. Melançon, Distinct functions for Arf guanine nucleotide exchange factors at the Golgi complex: GBF1 and BIGs are required for assembly and maintenance of the Golgi stack and trans-Golgi network, respectively. *Mol. Biol. Cell* **19**, 523–535 (2008).
11. A. Nawrotek, M. Zeghouf, J. Cherfils, Allosteric regulation of Arf GTPases and their GEFs at the membrane interface. *Small GTPases* **7**, 283–296 (2016).
12. J. M. Bhatt *et al.*, Promiscuity of the catalytic Sec7 domain within the guanine nucleotide exchange factor GBF1 in ARF activation, Golgi homeostasis, and effector recruitment. *Mol. Biol. Cell* **30**, 1523–1535 (2019).
13. T. Ogawa, M. Vatta, B. G. Bruneau, A. J. de Bold, Characterization of natriuretic peptide production by adult heart atria. *Am. J. Physiol.* **276**, H1977–H1986 (1999).
14. M. B. De Young, J. C. Keller, R. M. Graham, G. M. Wildey, Brefeldin A defines distinct pathways for atrial natriuretic factor secretion in neonatal rat atrial and ventricular myocytes. *Circ. Res.* **74**, 33–40 (1994).
15. E. Muth, W. J. Driscoll, A. Smalstig, G. Goping, G. P. Mueller, Proteomic analysis of rat atrial secretory granules: A platform for testable hypotheses. *Biochim. Biophys. Acta* **1699**, 263–275 (2004).
16. P. J. O'Donnell, W. J. Driscoll, N. Back, E. Muth, G. P. Mueller, Peptidylglycine-alpha-amidating monooxygenase and pro-atrial natriuretic peptide constitute the major membrane-associated proteins of rat atrial secretory granules. *J. Mol. Cell. Cardiol.* **35**, 915–922 (2003).
17. D. Kumar, R. E. Mains, B. A. Eipper, 60 Years of POMC: From POMC and α-MSH to PAM, molecular oxygen, copper, and vitamin C. *J. Mol. Endocrinol.* **56**, T63–T76 (2016).
18. V. Labrador, C. Brun, S. König, A. Roatti, A. J. Baertschi, Peptidyl-glycine alpha-amidating monooxygenase targeting and shaping of atrial secretory vesicles: Inhibition by mutated N-terminal ProANP and PBA. *Circ. Res.* **95**, e98–e109 (2004).
19. A. Menon *et al.*, Electrophysiologic and molecular mechanisms of a frameshift NPPA mutation linked with familial atrial fibrillation. *J. Mol. Cell. Cardiol.* **132**, 24–35 (2019).
20. N. N. Louros *et al.*, An N-terminal pro-atrial natriuretic peptide (NT-proANP) "aggregation-prone" segment involved in isolated atrial amyloidosis. *FEBS Lett.* **588**, 52–57 (2014).
21. V. Steinthorsdottir *et al.*, Identification of low-frequency and rare sequence variants associated with elevated or reduced risk of type 2 diabetes. *Nat. Genet.* **46**, 294–298 (2014).
22. A. Xue *et al.*; eQTLGen Consortium, Genome-wide association analyses identify 143 risk variants and putative regulatory mechanisms for type 2 diabetes. *Nat. Commun.* **9**, 2941 (2018).
23. W. Zhao *et al.*; CHD Exome+ Consortium; EPIC-CVD Consortium; EPIC-Interact Consortium; Michigan Biobank, Identification of new susceptibility loci for type 2 diabetes and shared etiological pathways with coronary heart disease. *Nat. Genet.* **49**, 1450–1457 (2017).
24. H. J. Yoo *et al.*, The peptidylglycine-α-amidating monooxygenase (PAM) gene rs13175330 A>G polymorphism is associated with hypertension in a Korean population. *Hum. Genomics* **11**, 29 (2017).

25. L. Jungk, H. Franke, A. Salameh, S. Dhein, Golgi fragmentation in human patients with chronic atrial fibrillation: A new aspect of remodeling. *Thorac. Cardiovasc. Surg.* **67**, 98–106 (2019).

26. S. Brandenburg, E. C. Arakel, B. Schwappach, S. E. Lehnart, The molecular and functional identities of atrial cardiomyocytes in health and disease. *Biochim. Biophys. Acta* **1863**, 1882–1893 (2016).

27. A. S. Go et al., Prevalence of diagnosed atrial fibrillation in adults: National implications for rhythm management and stroke prevention: The AnTicoagulation and Risk Factors in Atrial Fibrillation (ATRIA) Study. *JAMA* **285**, 2370–2375 (2001).

28. R. Agah et al., Gene recombination in postmitotic cells. Targeted expression of Cre recombinase provokes cardiac-restricted, site-specific rearrangement in adult ventricular muscle in vivo. *J. Clin. Invest.* **100**, 169–179 (1997).

29. E. H. Bossen, J. R. Sommer, R. A. Waugh, Comparative stereology of mouse atria. *Tissue Cell* **13**, 71–77 (1981).

30. N. Bäck et al., The endocytic pathways of a secretory granule membrane protein in HEK293 cells: PAM and EGF traverse a dynamic multivesicular body network together. *Eur. J. Cell Biol.* **96**, 407–417 (2017).

31. N. Bäck, C. Rajagopal, R. E. Mains, B. A. Eipper, Secretory granule membrane protein recycles through multivesicular bodies. *Traffic* **11**, 972–986 (2010).

32. R. E. Smith, M. G. Farquhar, Lysosome function in the regulation of the secretory process in cells of the anterior pituitary gland. *J. Cell Biol.* **31**, 319–347 (1966).

33. D. Bousquet-Moore et al., Reversal of physiological deficits caused by diminished levels of peptidylglycine α-amidating monooxygenase by dietary copper. *Endocrinology* **150**, 1739–1747 (2009).

34. J. W. Slot et al., Glucose transporter (GLUT-4) is targeted to secretory granules in rat atrial cardiomyocytes. *J. Cell Biol.* **137**, 1243–1254 (1997).

35. V. K. Rao, G. Zavala, A. Deb Roy, R. E. Mains, B. A. Eipper, A pH-sensitive luminal His-cluster promotes interaction of PAM with V-ATPase along the secretory and endocytic pathways of peptidergic cells. *J. Cell. Physiol.* **234**, 8683–8697 (2019).

36. M. R. Alam et al., Novel proteins that interact with the COOH-terminal cytosolic routing determinants of an integral membrane peptide-processing enzyme. *J. Biol. Chem.* **271**, 28636–28640 (1996).

37. G. Thibault et al., The propeptide Asn1-Tyr126 is the storage form of rat atrial natriuretic factor. *Biochem. J.* **241**, 265–272 (1987).

38. A. J. de Bold, Tissue fractionation studies on the relationship between an atrial natriuretic factor and specific atrial granules. *Can. J. Physiol. Pharmacol.* **60**, 324–330 (1982).

39. A. M. Oyarce, B. A. Eipper, Identification of subcellular compartments containing peptidylglycine alpha-amidating monooxygenase in rat anterior pituitary. *J. Cell Sci.* **108**, 287–297 (1995).

40. L. Ouafik, V. May, H. T. Keutmann, B. A. Eipper, Developmental regulation of peptidylglycine alpha-amidating monooxygenase (PAM) in rat heart atrium and ventricle. Tissue-specific changes in distribution of PAM activity, mRNA levels, and protein forms. *J. Biol. Chem.* **264**, 5839–5845 (1989).

41. X. Siebert et al., The catalytic copper of peptidylglycine alpha-hydroxylating monooxygenase also plays a critical structural role. *Biophys. J.* **89**, 3312–3319 (2005).

42. J. Palermo, J. Gulick, M. Colbert, J. Fewell, J. Robbins, Transgenic remodeling of the contractile apparatus in the mammalian heart. *Circ. Res.* **78**, 504–509 (1996).

43. C. Dorrell et al., Transcriptomes of the major human pancreatic cell types. *Diabetologia* **54**, 2832–2844 (2011).

44. H. Katsuta et al., Single pancreatic beta cells co-express multiple islet hormone genes in mice. *Diabetologia* **53**, 128–138 (2010).

45. S. Doroudgar et al., Hrd1 and ER-associated protein degradation, ERAD, are critical elements of the adaptive ER stress response in cardiac myocytes. *Circ. Res.* **117**, 536–546 (2015).

46. J. K. Jin et al., ATF6 decreases myocardial ischemia/reperfusion damage and links ER stress and oxidative stress signaling pathways in the heart. *Circ. Res.* **120**, 862–875 (2017).

47. C. Zhang et al., Unfolded protein response plays a critical role in heart damage after myocardial ischemia/reperfusion in rats. *PLoS One* **12**, e0179042 (2017).

48. E. Lau et al., Integrated omics dissection of proteome dynamics during cardiac remodeling. *Nat. Commun.* **9**, 120 (2018).

49. T. R. Gibson, P. P. Shields, C. C. Glembotski, The conversion of atrial natriuretic peptide (ANP)-(1-126) to ANP-(99-126) by rat serum: Contribution to ANP cleavage in isolated perfused rat hearts. *Endocrinology* **120**, 764–772 (1987).

50. P. P. Shields, C. C. Glembotski, The post-translational processing of rat pro-atrial natriuretic factor by primary atrial myocyte cultures. *J. Biol. Chem.* **263**, 8091–8098 (1988).

51. T. A. Thibaudeau, D. M. Smith, A practical review of proteasome pharmacology. *Pharmacol. Rev.* **71**, 170–197 (2019).

52. T. Ogawa, A. J. de Bold, The heart as an endocrine organ. *Endocr. Connect.* **3**, R31–R44 (2014).

53. H. Iida, Y. Shibata, Phasic secretion of newly synthesized atrial natriuretic factor from unstimulated atrial myocytes in culture. *Circ. Res.* **74**, 659–668 (1994).

54. A. A. Rauscher, M. Gyimesi, M. Kovács, A. Málnási-Csizmadia, Targeting myosin by blebbistatin derivatives: Optimization and pharmacological potential. *Trends Biochem. Sci.* **43**, 700–713 (2018).

55. A. J. Kee et al., ER/Golgi trafficking is facilitated by unbranched actin filaments containing Tpm4.2. *Cytoskeleton (Hoboken)* **74**, 379–389 (2017).

56. R. Vazhappilly, K. S. Wee, N. J. Sucher, C. M. Low, A non-muscle myosin II motor links NR1 to retrograde trafficking and proteasomal degradation in PC12 cells. *Neurochem. Int.* **56**, 569–576 (2010).

57. L. H. Hansen et al., Discovery of O-glycans on atrial natriuretic peptide (ANP) that affect both its proteolytic degradation and potency at its cognate receptor. *J. Biol. Chem.* **294**, 12567–12578 (2019).

58. A. J. Baertschi et al., Acid prohormone sequence determines size, shape, and docking of secretory vesicles in atrial myocytes. *Circ. Res.* **89**, E23–E29 (2001).

59. W. Han, Y. K. Ng, D. Axelrod, E. S. Levitan, Neuropeptide release by efficient recruitment of diffusing cytoplasmic secretory vesicles. *Proc. Natl. Acad. Sci. U.S.A.* **96**, 14577–14582 (1999).

60. R. El Meskini et al., A signal sequence is sufficient for green fluorescent protein to be routed to regulated secretory granules. *Endocrinology* **142**, 864–873 (2001).

61. A. M. Bourke, A. B. Bowen, M. J. Kennedy, New approaches for solving old problems in neuronal protein trafficking. *Mol. Cell. Neurosci.* **91**, 48–66 (2018).

62. R. Sannerud et al., Rab1 defines a novel pathway connecting the pre-Golgi intermediate compartment with the cell periphery. *Mol. Biol. Cell* **17**, 1514–1526 (2006).

63. L. Canaff, V. Brechler, T. L. Reudelhuber, G. Thibault, Secretory granule targeting of ANP correlates with its calcium-mediated aggregation. *Proc. Natl. Acad. Sci. U.S.A.* **93**, 9483–9487 (1996).

64. A. O. Jorgensen, A. C. Shen, K. P. Campbell, Ultrastructural localization of calsequestrin in adult rat atrial and ventricular muscle cells. *J. Cell Biol.* **101**, 257–268 (1985).

65. A. Nori, E. Bortoloso, F. Frasson, G. Valle, P. Volpe, Vesicle budding from endoplasmic reticulum is involved in calsequestrin routing to sarcoplasmic reticulum of skeletal muscles. *Biochem. J.* **379**, 505–512 (2004).

66. A. G. Grieve, C. Rabouille, Golgi bypass: Skirting around the heart of classical secretion. *Cold Spring Harb. Perspect. Biol.* **3**, a005298 (2011).

67. J. Béthune, F. T. Wieland, Assembly of COPI and COPII vesicular coat proteins on membranes. *Annu. Rev. Biophys.* **47**, 63–83 (2018).

68. K. Kurokawa, A. Nakano, The ER exit sites are specialized ER zones for the transport of cargo proteins from the ER to the Golgi apparatus. *J. Biochem.* **165**, 109–114 (2019).

69. K. Saegusa, M. Sato, N. Morooka, T. Hara, K. Sato, SFT-4/Surf4 control ER export of soluble cargo proteins and participate in ER exit site organization. *J. Cell Biol.* **217**, 2073–2085 (2018).

70. M. Bonnemaison et al., AP-1A controls secretory granule biogenesis and trafficking of membrane secretory granule proteins. *Traffic* **15**, 1099–1121 (2014).

71. M. R. Alam et al., Signaling mediated by the cytosolic domain of peptidylglycine alpha-amidating monooxygenase. *Mol. Biol. Cell* **12**, 629–644 (2001).

72. D. Kumar et al., Microvillar and ciliary defects in zebrafish lacking an actin-binding bioactive peptide amidating enzyme. *Sci. Rep.* **8**, 4547 (2018).

73. J. B. Dacks, M. S. Robinson, Outerwear through the ages: Evolutionary cell biology of vesicle coats. *Curr. Opin. Cell Biol.* **47**, 108–116 (2017).

74. G. D. Ciccotosto, M. R. Schiller, B. A. Eipper, R. E. Mains, Induction of integral membrane PAM expression in AtT-20 cells alters the storage and trafficking of POMC and PC1. *J. Cell Biol.* **144**, 459–471 (1999).

75. F. Pluteanu et al., Progressive impairment of atrial myocyte function during left ventricular hypertrophy and heart failure. *J. Mol. Cell. Cardiol.* **114**, 253–263 (2018).

76. F. Bisbal, A. Baranchuk, E. Braunwald, A. Bayés de Luna, A. Bayés-Genís, Atrial failure as a clinical entity: JACC review topic of the week. *J. Am. Coll. Cardiol.* **75**, 222–232 (2020).

77. S. Dhein et al., Mechanical control of cell biology. Effects of cyclic mechanical stretch on cardiomyocyte cellular organization. *Prog. Biophys. Mol. Biol.* **115**, 93–102 (2014).

78. D. R. Caprette, M. L. Entman, W. B. Van Winkle, Association of clathrin with microsomes isolated from canine myocardium. *Circ. Res.* **58**, 120–126 (1986).

79. I. Belevich, M. Joensuu, D. Kumar, H. Vihinen, E. Jokitalo, Microscopy image browser: A platform for segmentation and analysis of multidimensional Datasets. *PLoS Biol.* **14**, e1002340 (2016).

80. J. Guo, W. Wang, D. Yu, Y. Wu, Spinoculation triggers dynamic actin and cofilin activity that facilitates HIV-1 infection of transformed and resting CD4 T cells. *J. Virol.* **85**, 9824–9833 (2011).

CELL BIOLOGY

Bäck et al.

www.manaraa.com